

Weekly rhythms of urban heat islands: A multicity perspective

Huilin Du^a, Wenfeng Zhan^{a,b,*}, Zihan Liu^a, Chunli Wang^a, Shasha Wang^a, Long Li^a, Jiufeng Li^a, Benjamin Bechtel^c, Panagiotis Sismanidis^c

^a Jiangsu Provincial Key Laboratory of Geographic Information Science and Technology, International Institute for Earth System Science, Nanjing University, Nanjing, Jiangsu 210023, China

^b Jiangsu Center for Collaborative Innovation in Geographical Information Resource Development and Application, Nanjing, Jiangsu 210023, China

^c Department of Geography, Ruhr-University Bochum, Bochum, Nordrhein-Westfalen 44801, Germany



ARTICLE INFO

Keywords:

Canopy urban heat island
Surface urban heat island
Thermal remote sensing
Weekly rhythms
Human activity variations

ABSTRACT

Investigating the weekly rhythms of urban heat islands (UHIs) is critical for gaining deep insights into the urban climate changes caused by periodic cycles of human activities. However, the weekly rhythms of both canopy and surface UHIs (termed I_c and I_s) remain poorly understood at a large spatial scale. Leveraging daily screen-level air temperature (T_a) and satellite land surface temperature (T_s) observations (2015–2020), we show that the weekly rhythms of I_c averaged for all selected cities exhibit an evident peak-and-valley pattern across most seasons, with the annual mean I_c reduction during weekends of 0.09 ± 0.01 K (mean \pm S.E., $p < 0.05$) for daytime and 0.10 ± 0.01 K ($p < 0.05$) for nighttime when compared to weekdays. In contrast, the I_s only displays a pronounced weekly rhythm during winter daytime, with the corresponding I_s reduction during weekends of 0.07 ± 0.01 K ($p < 0.05$) relative to weekdays. These findings remain robust against potential observation errors in T_a and T_s . From an intra-city perspective, both I_c and I_s reductions during weekends escalate with increasing urban impervious surface percentage. This study illustrates the significance of short-term cycles of human activities in shaping global urban climates.

1. Introduction

Human activities within cities have significantly reshaped the urban surface energy budget, leading to noteworthy alterations in local and regional climates (Oke, Mills, Christen & Voogt, 2017). Among these alterations, the urban heat island (UHI) effect emerges as a critical concern due to its profound implications for public health, energy consumption, and urban eco-environments (Hsu, Sheriff, Chakraborty & Manya, 2021; Santamouris, 2014; Shen et al., 2022; Zhang et al., 2023; Zhao et al., 2018). Human activities in cities typically follow a regular weekly schedule (Earl, Simmonds & Tapper, 2016), which can lead to weekly rhythms of anthropogenic heat releases (AHR), a pivotal component of the urban surface energy budget (Oke et al., 2017), further triggering the weekly rhythms of UHI (Wang et al., 2022a).

Canopy UHI (I_c), quantified by screen-level air temperature (T_a), and surface UHI (I_s), assessed through land surface temperature (T_s), represent two critical types of UHI (Oke, 1973; Venter, Chakraborty & Lee, 2021; Wu et al., 2022; Yang et al., 2023). From an urban climatology perspective, these two types of UHI are influenced by AHR in

distinct ways. Specifically, AHR can directly warm the air layer and enhance canopy UHI, while it can also affect other components of the urban surface energy budget (such as sensible heat) and directly influence surface UHI through urban surface-atmosphere interactions (Oke et al., 2017; Shahmohamadi, Che-Ani, Maulud, Tawil & Abdullah, 2011). Investigations into the weekly rhythms of both I_c and I_s are expected to help better understand the modulation of AHR on urban climates.

Existing studies have primarily relied on *in-situ* T_a measurements to examine the weekly rhythms of canopy UHI in individual cities, with little attention paid to surface UHI. This inclination of previous investigations is attributed to the traditional practice among climatologists of analyzing the weekly rhythms of T_a to discern anthropogenic impacts and more precisely monitor global warming (Forster & Solomon, 2003; Gong, Guo & Ho, 2006). In recent years, with increasing attention directed towards urban climates, practitioners have begun investigating the differences in the weekend effect of T_a between urban and rural surfaces, aiming to highlight the significant influence of human activities within cities on urban climates. Observational evidences from cities located in cold climates have generally reached a

* Corresponding author at: Nanjing University at Xianlin Campus, No. 163 Xianlin Avenue, Qixia District, Nanjing, Jiangsu 210023, China.
E-mail address: zhanwenfeng@nju.edu.cn (W. Zhan).

Abbreviations and symbols	
AHR	anthropogenic heat release
ISP	impervious surface percentage
UHI	urban heat island
WD	weekday, defined as Monday to Friday
WE	weekend, defined as Saturday and Sunday
I_c	canopy UHI intensity, quantified as urban-rural contrast in screen-level air temperature
I_{c_time}	daily I_c from Monday to Sunday
I_{c_mean}	weekly average I_c
I_s	surface UHI intensity, quantified as urban-rural contrast in land surface temperature
I_{s_time}	daily I_s from Monday to Sunday
I_{s_mean}	weekly average I_s
T_a	screen-level air temperature
T_{a_WD}	T_a at weekdays
T_{a_WE}	T_a at weekends
T_s	land surface temperature
T_{s_WD}	T_s at weekdays
T_{s_WE}	T_s at weekends
ΔI_c	the differences in I_c between weekends and weekdays
ΔI_s	the differences in I_s between weekends and weekdays
ΔI_{c_day}	daytime ΔI_c
ΔI_{c_ngt}	nighttime ΔI_c
ΔI_{s_day}	daytime ΔI_s
ΔI_{s_ngt}	nighttime ΔI_s
ΔI_{ano_c}	I_c anomaly, calculated as the daily I_c minus the weekly average
ΔI_{ano_s}	I_s anomaly, calculated as the daily I_s minus the weekly average
$\Delta I_{ano_c_day}$	daytime ΔI_{ano_c}
$\Delta I_{ano_c_ngt}$	nighttime ΔI_{ano_c}
$\Delta I_{ano_s_day}$	daytime ΔI_{ano_s}
$\Delta I_{ano_s_ngt}$	nighttime ΔI_{ano_s}
ΔT_a	the differences in T_a between weekends and weekdays
ΔT_s	the differences in T_s between weekends and weekdays
ΔT_{a_u}	ΔT_a for urban stations
ΔT_{a_r}	ΔT_a for rural stations
ΔT_{s_u}	ΔT_s for urban surfaces
ΔT_{s_r}	ΔT_s for rural surfaces

consensus – the I_c is significantly lower during weekends (usually defined as Saturday and Sunday) than weekdays (Monday to Friday) (Ngarambe, Joen, Han & Yun, 2021; Wang et al., 2022a). However, for cities in equatorial and temperate climates, conclusions remain often contradictory – most studies have observed a weakened I_c during weekends due to notable reductions in AHR (Earl et al., 2016; Kamma et al., 2020; Nwaerema & Jiya, 2021; Papanastasiou & Kittas, 2012), while others have reported an amplified weekend I_c when compared with weekdays (Elsayed, 2012). These disparities may arise from differences in study periods and the used methods. Regarding diurnal and seasonal variations, the I_c reduction (termed ΔI_c , expressed as the I_c difference between weekends and weekdays) is typically more pronounced at night than during the day and more substantial in winter than in summer (Earl et al., 2016; Papanastasiou & Kittas, 2012; Wang et al., 2022a). Besides, a more evident I_c reduction during weekends was often observed over urban surfaces with a higher impervious surface percentage (ISP), especially at night (Wang et al., 2022a).

Despite the progresses achieved by previous studies, three lingering questions remain. Firstly, previous studies on the weekly rhythms of canopy UHI are mostly confined to individual cities, and their obtained conclusions are often contradictory. It remains unclear to what extent the I_c exhibits a weekly rhythm at a relatively large spatial scale encompassing cities with diverse geographical and climatic contexts. Secondly, in addition to I_c , the I_s is also anticipated to be influenced by weekly schedules of anthropogenic activities within cities, yet its weekly rhythms, to the best of our knowledge, have never been examined so far even at the city-scale. Finally, it remains vague whether the high correlation between ΔI_c and ISP inferred from individual cities can be extrapolated to a broader scale for both ΔI_c and ΔI_s (i.e., the I_s difference between weekends and weekdays).

To address these gaps, here we investigate the spatiotemporal patterns of the weekly rhythms of both canopy and surface UHIs from a multicity perspective, by combining daily *in-situ* T_a measurements retrieved from >17,000 weather stations and satellite-derived T_s observations worldwide from 2015 to 2020. We further employ the ISP as an indicator of urban surface property and analyze its relationship with both ΔI_c and ΔI_s to better discern their intra-city patterns. We need to note that the main intention of our study is not to compare the ΔI_c and ΔI_s patterns under uniform criteria, but rather to (1) extend the local results of ΔI_c to a larger spatial scale and provide a holistic view of the ΔI_c pattern, and (2) provide the first assessment of the weekly rhythms

of surface UHI.

2. Study area and data

2.1. Study area

We selected a total of 743 and 988 cities worldwide (each with an urban area of > 5 km² in 2000; Fig. 1) for the investigation of weekly rhythms of canopy and surface UHIs, respectively. These two categories of cities were chosen based on the data quality of T_a and T_s observations within cities (refer to Section 3.2). According to the Köppen–Geiger climate classification system (Peel, Finlayson & McMahon, 2007), the 743 cities used for ΔI_c investigation are distributed in equatorial (8 cities), arid (116 cities), warm (297 cities) and cold (322 cities) climates. These cities are unevenly distributed worldwide owing to the highly uneven distribution of weather stations (Figs. A1 and A2). We acknowledge that such uneven distribution of the chosen cities may introduce potential uncertainties into the quantification of ΔI_c due to the insufficient representativeness of global cities. Further discussions regarding this issue are provided in Section 5.2. The 988 cities used for ΔI_s investigation are abundantly distributed in equatorial (144 cities), arid (140 cities), warm (557 cities), and cold (147 cities) climates.

2.2. Data

We employed meteorological data, MODIS data, and auxiliary data for analysis. The meteorological data comprised daily maximum and minimum *in-situ* T_a measurements from 2015 to 2020 and were sourced from two datasets. We primarily utilized T_a measurements from > 15,000 weather stations worldwide provided by the Global Historical Climatology Network Daily datasets (Menne, Durre, Vose, Gleason & Houston, 2012; available at: <https://www.ncdc.noaa.gov/pub/data/ghcn/daily/>). Given the relatively sparse distribution of these stations across China, we further leveraged the T_a measurements over 2419 stations from China Meteorological Data Service centre (Cao, Zhu, Tang, Yuan & Yan, 2016; available at: <http://data.cma.cn/>). Both of these sources have been widely utilized within the urban climate community (Du et al., 2021; Zhang et al., 2021; Zhou, Sun, Li, Zhang & Huang, 2023). To ensure the reliability of the data, we further performed data homogenization tests for both meteorological datasets using the RHtestV4 method (Luo & Lau, 2019; Wang, 2008; Zhang et al., 2021),

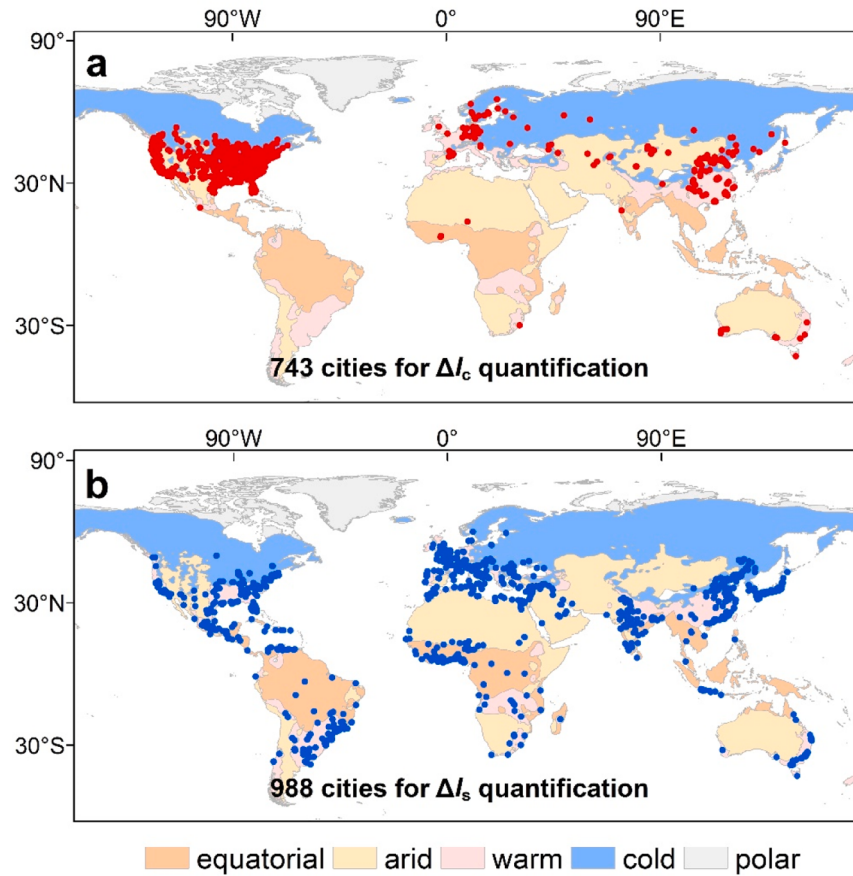


Fig. 1. Distribution of the 743 and 988 cities used for ΔI_c (a) and ΔI_s (b) investigation.

and retained only stations with homogeneous T_a measurements for further analysis.

The MODIS data encompassed daily T_s observations provided by MYD11A1 (with a spatial resolution of 1 km) and yearly land cover type data obtained from MCD12Q1 (500 m). The MYD11A1 dataset can provide spatially continuous and periodic T_s observations, and it has been extensively employed in previous studies (Chakraborty & Lee, 2019; Li et al., 2013; Peng et al., 2012). Here we employed the daytime and nighttime T_s observations from 2015 to 2020 to investigate the weekly rhythms of global surface UHI. Noting that the MYD11A1 product rather than MOD11A1 product was leveraged here mainly because the observation times of daytime and nighttime T_s provided by MYD11A1 are closer to those of daily maximum and minimum *in-situ* T_a observations when compared with the MOD11A1 counterpart (Oke et al., 2017). The land cover type data provided by the International Geosphere-Biosphere Program scheme were used to eliminate pixels such as wetlands, water, and snow and ice (Friedl & Sulla Menashe, 2019), and these data were resampled to 1 km.

The auxiliary data consisted of global urban boundary (GUB) data, global artificial impervious area (GAIA) data, and elevation data (GTOPO30). The GUB data involve all the urban boundaries and human settlements with area exceeding 1 km² (Li et al., 2020). Here the GUB data in the year 2000 and 2018 were employed to delineate urban and rural surfaces. The GAIA data provide the global impervious surfaces from 1985 to 2018 and they are characterized by a spatial resolution of 30 m (Gong et al., 2020). We utilized the GAIA data to identify urban and rural stations as well as to examine the relationships between urban ISP and ΔI across global cities. The elevation data hold a spatial resolution of 30 arc minutes and were resampled to 1 km. We employed such data to exclude pixels with elevation exceeding ± 50 m of the median elevation of all urban pixels in each city (Imhoff, Zhang, Wolfe &

Bounoua, 2010).

3. Methods

3.1. Delineation of urban and rural areas and stations

Urban surfaces closer to the city center typically experience more intensive human activities compared to those situated on the urban periphery. As a result, these central surfaces are expected to demonstrate more pronounced weekly cycles of human activities (Wang et al., 2022a). In light of this, we defined the urban area as the surfaces located within the urban boundary in the year 2000, according to the GUB dataset provided by Li et al. (2020) (refer to Section 2.2). We further delineated the rural backgrounds as the buffer ring between the 10-km and 100-km buffer zones outside the urban boundary in the year 2018 (Fig. A3; Du et al., 2023; Luo & Lau, 2018). To quantify the I_s and I_c more accurately, we further excluded the pixels labelled as wetlands, water, and snow and ice owing to their notably lower temperatures (Lai et al., 2018; Peng et al., 2012). We also discarded the pixels with elevation beyond ± 50 m of the median elevation of each city (Imhoff et al., 2010; Venter et al., 2021).

We classified all stations into urban or rural categories according to their geographical locations and the surrounding ISPs within the 1-km buffer zone. The 1-km buffer zone was used mainly because meteorological sensors generally capture the ambient weather conditions within 1-km (Oke, 2004). The surrounding ISP for each station was determined by calculating the proportion of impervious surface area accounting for the total area of 1-km buffer zone based on the 30-m GAIA product (Zhou et al., 2023). On this basis, we designated stations as urban if they were located within the urban boundary and possessed a surrounding ISP larger than 20%. Similarly, we identified rural stations as those

situated within rural surroundings and with a surrounding ISP less than 5%. The threshold of 20% was employed for the delineation of urban stations mainly because it typically distinguishes between low-density urban surfaces and rural surfaces (Song, Sexton, Huang, Channan & Townshend, 2016). Stations with surrounding ISPs ranging between 5% and 20% were not involved in the rural category mainly to screen out the very pure rural stations (Oke et al., 2017).

3.2. Quantification and investigation of the weekly rhythms of I_c and I_s

Regarding the weekly rhythms of I_c , we adhered to the following procedures to perform quality control of *in-situ* T_a measurements. Firstly, daily maximum T_a must be larger than daily minimum T_a for any given day (Forster & Solomon, 2003). We therefore ruled out the observation days with daily minimum T_a anomalously larger than daily maximum T_a to eliminate the impacts from data inconsistency on the quantification of ΔI_c . Secondly, to mitigate possible impacts arising from data anomalies, we calculated the mean (μ) and standard deviation (σ) of the daily time series T_a for each station, and discarded the days with T_a measurements falling outside the range of $\mu - 3\sigma$ to $\mu + 3\sigma$. Thirdly, we filtered out stations with a data missing rate exceeding one third throughout the study period to suppress potential uncertainties induced by missing data. Considering that approximately 3% of the stations across North America only provide T_a measurements during weekdays probably due to the operator biases (Forster & Solomon, 2003), we further only retained the stations with a missing data rate less than 50% during both weekends and weekdays across all seasons to minimize the effects stemming from operator biases. Given the scarcity of eligible stations across the equatorial climate zone (mainly located in economically underdeveloped regions of Latin America and Africa), we slightly loosened the city selection criteria for this region – stations with a data missing rate less than 90% throughout the study period were included for further analysis. These quality control criteria for T_a measurements allowed us to finally pick out 1068 urban stations and 1884 rural stations that cover 743 cities worldwide for the investigation of weekly rhythms of canopy UHI (Fig. 1a and Fig. A2).

Regarding the weekly rhythms of I_s , we employed the following procedures to filter satellite-derived T_s observations. To minimize the impacts from data deficiency of T_s products, we first picked out the pixels with retrieval error of less than 2.0 K based on the quality control band of MODIS T_s products (Venter et al., 2021). Subsequently, we screened the pixels with a data missing rate lower than 80% during both weekends and weekdays throughout the study period to suppress the uncertainties related to the missing records induced by cloud contaminations (Liu et al., 2022). On this basis, we disregarded the cities with valid pixel number less than 5, and finally chosen a total of 988 cities worldwide for the investigation of the weekly rhythms of I_s (Fig. 1b).

We employed the anomalies of I_c and I_s (i.e., $\Delta I_{ano,c}$ and $\Delta I_{ano,s}$; quantified as the daily I_c or I_s minus the weekly average; Table 1) to portray the patterns of the weekly rhythms of canopy and surface UHIs, respectively. We further quantified the difference in I_c (or I_s) between weekends and weekdays, also known as the weekend effect of UHI (i.e., ΔI_c and ΔI_s ; Earl et al., 2016), to characterize the variation magnitude of the weekly rhythms of I_c (or I_s). Specifically, we first calculated the

weekend effect of T_a (or T_s) over both urban and rural surfaces (termed ΔT_a or ΔT_s), and then estimated the ΔI_c (or ΔI_s) as the mean ΔT_a (or ΔT_s) difference between urban and rural surfaces (Table 1).

Considering the diverse patterns of I_c and I_s across various temporal and spatial scales (Chakraborty & Lee, 2019; Peng et al., 2012), we examined the diurnal and seasonal variations of ΔI_c and ΔI_s , as well as their variations across different climate zones and continents. Here we only involved the climate zones and continents with more than 5 valid cities for statistical analyses. From an intra-city perspective, urban surfaces with higher ISP typically possess more intense human activity (Gong et al., 2020; Zhang et al., 2020), and consequently, these surfaces should experience a more pronounced reduction in human activity during weekends in comparison to those with lower ISP (Hart & Sailor, 2009; Wang et al., 2022a). To better discern the intra-city dynamics of ΔI_c and ΔI_s , we further examined their variations along with different ISPs across global cities. For our current study, spring, summer, autumn, and winter were defined as March to May, June to August, September to November, and December to February for northern hemispheric cities; and vice versa for southern hemispheric cities. The aforementioned analyses were predominantly conducted using Google Earth Engine (GEE) and Matlab.

3.3. Uncertainty analysis

There may exist some potential uncertainties in our study, including the uncertainties stemming from observation errors of T_a and T_s , daily variation of weather systems, and the involvement of official holidays.

Firstly, the quantification of ΔI_c pattern may be impacted by the observation error of *in-situ* T_a measurements (about 0.1 K). Similarly, the examination of ΔI_s pattern may be influenced by the retrieval error as well as other inherent limitations of satellite T_s observations (e.g., missing data due to cloud contaminations). Regarding these issues, we adopted an error injection strategy to examine the potential impacts from observations errors of T_a and T_s on the quantification of ΔI_c and ΔI_s . Specifically, for time-series T_a observations of each weather station, we first created a random error field with a mean of 0 and a standard deviation of 0.1 by generating random numbers (Buizza, Milleer & Palmer, 1999). Subsequently, we superimposed this random error field onto the original daily T_a observations to generate a new daily T_a time series. Leveraging such daily T_a time series perturbed by random error, we re-quantified the weekly rhythms of canopy UHI and compared them with the original results. Similarly, for satellite-derived T_s observations, we first generated an error image with a mean of 0 and a standard deviation of 1 by generating random numbers. We then added this image to the original daily T_s images and obtained new images with error perturbations. Using these newly generated daily T_s images, we re-quantified the weekly rhythms of surface UHI. Furthermore, we introduced the Bessel formula in error theory ($\frac{\delta}{\sqrt{n-1}}$, with n denoting the sample number and δ representing the observation error of *in-situ* T_a or the retrieval error of satellite-derived T_s ; Pugachev, 2014; Wang et al., 2022a; Ye, Xiao, Shi & Ling, 2016) to analyze these potential impacts from a mathematical perspective. The Bessel formula holds for our present study mainly because the observation errors are often considered to be random and independent (Zahumenský, 2004) and they also adhere to normal distribution according to the central limit theorem (Bonamente, 2017). For the weekly rhythms of I_s , we additionally conducted two sensitivity analyses. Firstly, we examined the impacts from T_s retrieval error by comparing the ΔI_s quantified using all pixels, pixels with a retrieval error of less than or equal to 3.0 K, and pixels with a retrieval error of less than or equal to 2.0 K, respectively. Secondly, we examined the impacts from data missing rate by comparing the ΔI_s quantified using pixels with the record number during both weekends and weekdays throughout the study period greater than 5%, 10%, 15%, and 20%, respectively.

Secondly, daily variations of weather systems may also introduce

Table 1
Calculation methods of the main variables used in this study.
The meaning of each variable is provided in Abbreviations and symbols.

Variable	Calculation
ΔT_a	$\Delta T_a = T_{a,WE} - T_{a,WD}$
ΔT_s	$\Delta T_s = T_{s,WE} - T_{s,WD}$
ΔI_c	$\Delta I_c = \Delta T_{a,u} - \Delta T_{a,r}$
ΔI_s	$\Delta I_s = \Delta T_{s,u} - \Delta T_{s,r}$
$\Delta I_{ano,c}$	$\Delta I_{ano,c} = I_{c,time} - I_{c,mean}$
$\Delta I_{ano,s}$	$\Delta I_{ano,s} = I_{s,time} - I_{s,mean}$

possible uncertainties into our analysis (Zhang et al., 2024). To examine these impacts, we generated a new T_a time-series by adding a series of random values that used to represent daily weather variations to the original T_a time series, and compared the ΔI_c calculated using the original and new T_a time series. Specifically, for each station, we first calculated the daily T_a fluctuation (termed A) by averaging the absolute values of T_a differences between all adjacent two days. We then generated a series of random values spanning the range from $-A$ to A and considered these values as the T_a fluctuations induced by daily weather variations. We finally added these random values to the original T_a time series and generated a new T_a time series (Buizza et al., 1999; Cryer & Chan, 2008). On this basis, we investigated the impacts from daily weather variation by comparing the ΔI_c calculated based on the original and the newly obtained T_a time series.

Thirdly, the involvement of official holidays may also impact the quantification of weekly rhythms of UHIs. Regarding this issue, we first identified all official holidays throughout the study period for each country using the Python's holiday library. Subsequently, we removed these holidays from all weekdays and re-quantified the ΔI_c patterns. We further examined the impacts from official holidays by comparing the ΔI_c quantified with or without considering such impacts.

4. Results

4.1. Weekly rhythms of I_c

The weekly rhythms of I_c , characterized by ΔI_{ano_c} (i.e., the daily I_c minus the weekly average), exhibited clear peak-and-valley patterns during both daytime and nighttime across all selected cities (Fig. 2c and d). The global mean daytime ΔI_{ano_c} demonstrated positive values from Monday through Thursday, while they turned into negative from Friday to Sunday, with the peak and valley occurring on Tuesday (0.13 K) and Saturday (-0.13 K), respectively. The global mean nighttime ΔI_{ano_c} displayed a similar pattern to that during the day, with a maximum of 0.15 K at Tuesday and a minimum of -0.12 K at Saturday. It is worth highlighting that the ΔI_{ano_c} was also notably negative at Friday (i.e., -0.07 K for both daytime and nighttime). We speculate that such a phenomenon does not matter much with the fact that Friday is a free day in Muslim countries, mainly owing to the relatively limited number of selected cities across these regions. By further investigating the number of urban stations characterized by negative ΔT_{ano_a} (i.e., daily T_a minus the weekly mean; Fig. A4), we speculate that such a negative ΔI_{ano_c} at Friday may be related to the significant reduction in human activity intensity in comparison to other weekdays across many regions of the world. Besides, the daily alternation of observers for some stations across North America does not consistently align with local midnight (Forster & Solomon, 2003), during which the maximum and minimum T_a measurements recorded on Fridays may occur at Saturdays (Menne et al., 2012). These may also be related to the observed negative ΔI_{ano_c} at Friday.

The annual mean daytime ΔI_c (i.e., the I_c difference between weekends and weekdays) reached $-0.09 \text{ K} \pm 0.01 \text{ K}$ (mean \pm standard error, $p < 0.05$), with 50% of the cities showing a negative daytime ΔI_c (Fig. 2a). The annual mean ΔI_c at night was $-0.10 \text{ K} \pm 0.01 \text{ K}$ ($p < 0.05$), and 54% of the cities exhibited a negative nighttime ΔI_c (Fig. 2b). These ΔI_c values aligned well with the findings of previous case studies that employed T_a measurements densely distributed within cities (e.g., -0.05 K for daytime and -0.13 K for nighttime reported in Wang et al., 2022a). These negative ΔI_c values could be attributed to the phenomenon that urban surfaces generally experience a more pronounced reduction in annual mean T_a during weekends in contrast to their rural counterparts (Fig. 3a), due to a more substantial decline in human activity-induced AHR (Earl et al., 2016). Besides, the slightly larger I_c reduction at night when compared with the day may be because that vertical air mixing is largely diminished during nighttime due to the absence of solar radiation, leading to the AHR concentration in

near-surface air layer and consequently an amplified AHR impact on I_c (Oke, 1982; Oke et al., 2017). Nevertheless, there were also a few cities exhibiting a positive ΔI_c , which may be ascribed to the combined impacts from AHR and aerosol reductions – the I_c enhancement induced by aerosol reduction during weekends may slightly outweigh the I_c decline induced by AHR reduction in these cities (refer to Section 5.1 for details).

From a seasonal perspective, both the daytime and nighttime ΔI_c reached the minimum (i.e., the largest I_c reduction) in autumn (-0.35 K during the day and -0.26 K at night; Fig. 4a and b; Figs. A5 and A6). During this season, urban surfaces witnessed noteworthy daytime and nighttime T_a reductions during weekends; comparably, their rural surroundings experienced a converse T_a increase (Fig. 3d). The ΔI_c at spring was less evident, characterized by the daytime ΔI_c of -0.09 K and the nighttime ΔI_c of -0.06 K (Fig. 4a and b). In spring, both urban and rural surfaces experienced T_a reductions during weekends, yet with the former more pronounced than the latter (Fig. 3b). The ΔI_c for winter was -0.004 K during the day and -0.10 K at night (Fig. 4a and b). While for summer, the ΔI_c was positive for both daytime (0.10 K) and nighttime (0.04 K). The summertime T_a over rural surfaces was greatly reduced during weekends for both daytime and nighttime, while the urban T_a was increased during the day and decreased slightly at night (Fig. 3c). This is likely attributed to the multifaceted interactions between aerosols and I_c . Specifically, solar radiation is most intense in summer, during which the reduction in aerosols during weekends could greatly enhance the solar radiation received by urban surfaces (refer to Section 5.1 for more details), thereby strengthening the I_c and leading to a positive ΔI_c .

From an intra-city perspective, we observed a strong correlation between ΔT_a and ISP at a global scale (Fig. 4c and d). During the day, the ΔT_a decreases from 0.04 K over low ISP surfaces (i.e., $ISP < 0.125$) to -0.08 K over high ISP surfaces (i.e., $ISP > 0.5$) (Fig. 4c). At night, the ΔT_a displayed a similar pattern with that during the day (Fig. 4d). The nighttime ΔT_a was 0.04 K for low ISP surfaces while reached as low as -0.05 K over highly urbanized surfaces (Fig. 4d). A more negative ΔT_a (i.e., a larger T_a reduction magnitude) over surfaces with higher ISP during both daytime and nighttime is mainly because these surfaces usually coincide with more pronounced reductions in human activity-induced AHR during weekends (Wang et al., 2022a).

The ΔI_c differed greatly by climate zones (Fig. 4e and f). During the day (Fig. 4e), the ΔI_c was most negative in cold climates (i.e., the largest I_c reduction; -0.11 K), followed by arid ($\Delta I_c = -0.09$ K) and warm climates ($\Delta I_c = -0.04$ K). Analogously, at night, the most pronounced I_c reductions were observed in cold and equatorial climates, characterized by the ΔI_c of -0.14 K and -0.11 K, respectively (Fig. 4f). The nighttime ΔI_c in both arid and warm climates was -0.06 K. The larger I_c reduction in cold climates for both daytime and nighttime could be attributed to the relatively larger AHR impacts on the I_c in these regions. Specifically, shortwave irradiance is considerably weaker for these mid- and high-latitude cities, thereby leading to a more dominant role of AHR in modulating the urban surface energy budget (Oke et al., 2017).

The ΔI_c was also distinctly different across continents (Fig. 4g and h). The most evident I_c reduction occurred in cities across North America regardless of time-of-day, with the ΔI_c of -0.11 K during the day and -0.13 K at night. In contrast, the ΔI_c for European cities was positive during the day (0.01 K) and slightly negative at night (-0.01 K). This may be related to the high degree of flexibility in the length and arrangement of working hours for European employees (Giachi & Vallejo-Peña, 2022), which leads to a less pronounced difference in human activities between weekdays and weekends. Besides, we suspect that the aerosol-cloud interaction may also contribute to the positive ΔI_c of European cities (refer to Section 5.1).

4.2. Weekly rhythms of I_s

Satellite-derived I_s across all selected cities only showed an evident

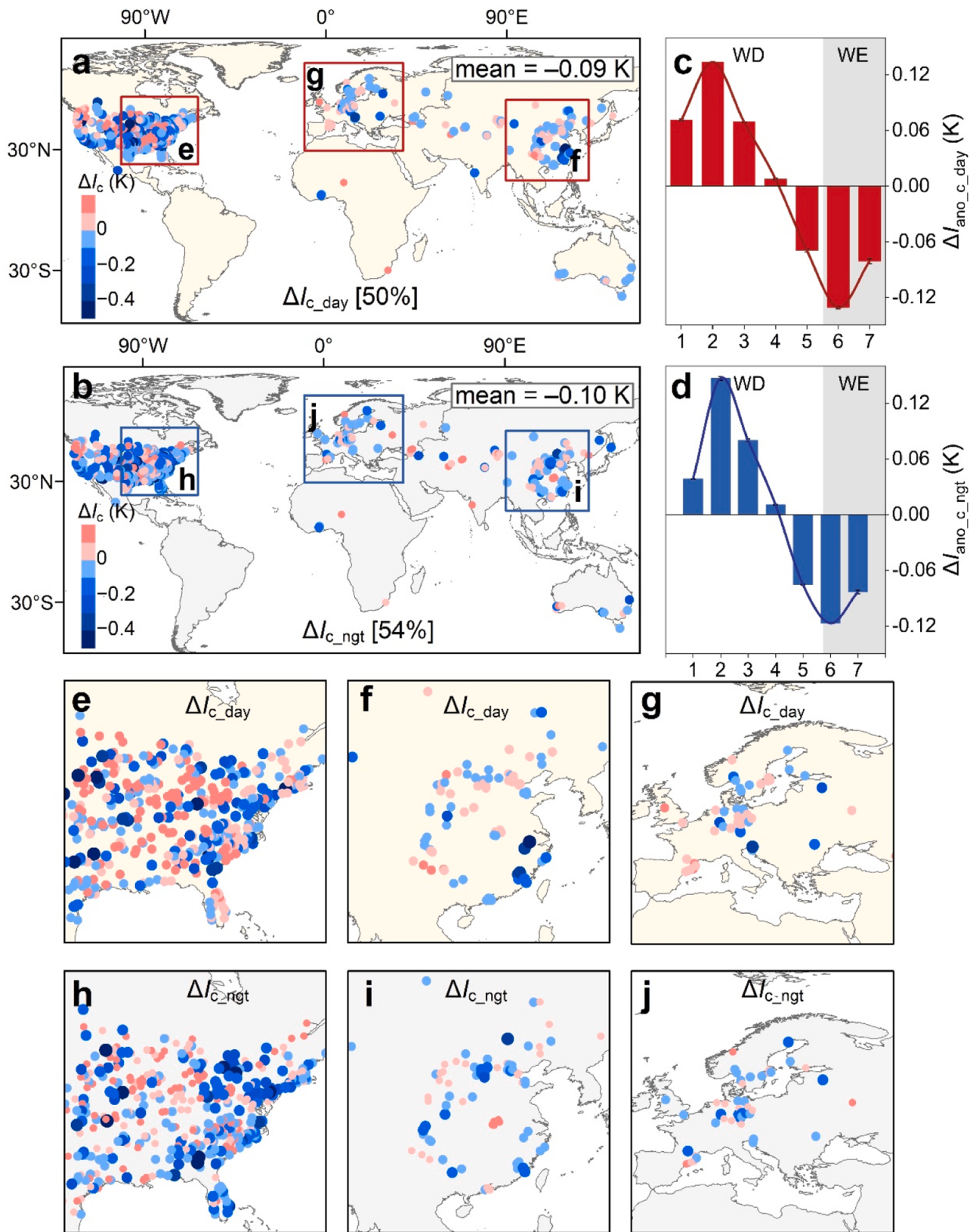


Fig. 2. Weekly rhythms of I_c across all selected cities | Spatial patterns of the weekend effect of I_c for daytime (ΔI_c_{day} ; a) and nighttime (ΔI_c_{ngt} ; b), with percentages in parentheses denoting the proportion of cities with a negative ΔI_c ; weekly rhythms of annual mean I_c (denoted by I_c anomalies, termed ΔI_{ano_c}) for daytime ($\Delta I_{\text{ano}_c_{\text{day}}}$; c) and nighttime ($\Delta I_{\text{ano}_c_{\text{ngt}}}$; d); the enlarged rectangular regions within (a) and (b) for daytime (e to g) and nighttime (h to j). WE and WD are abbreviations for weekends and weekdays respectively, and the numbers of 1 to 7 within (c) and (d) denote Monday to Sunday.

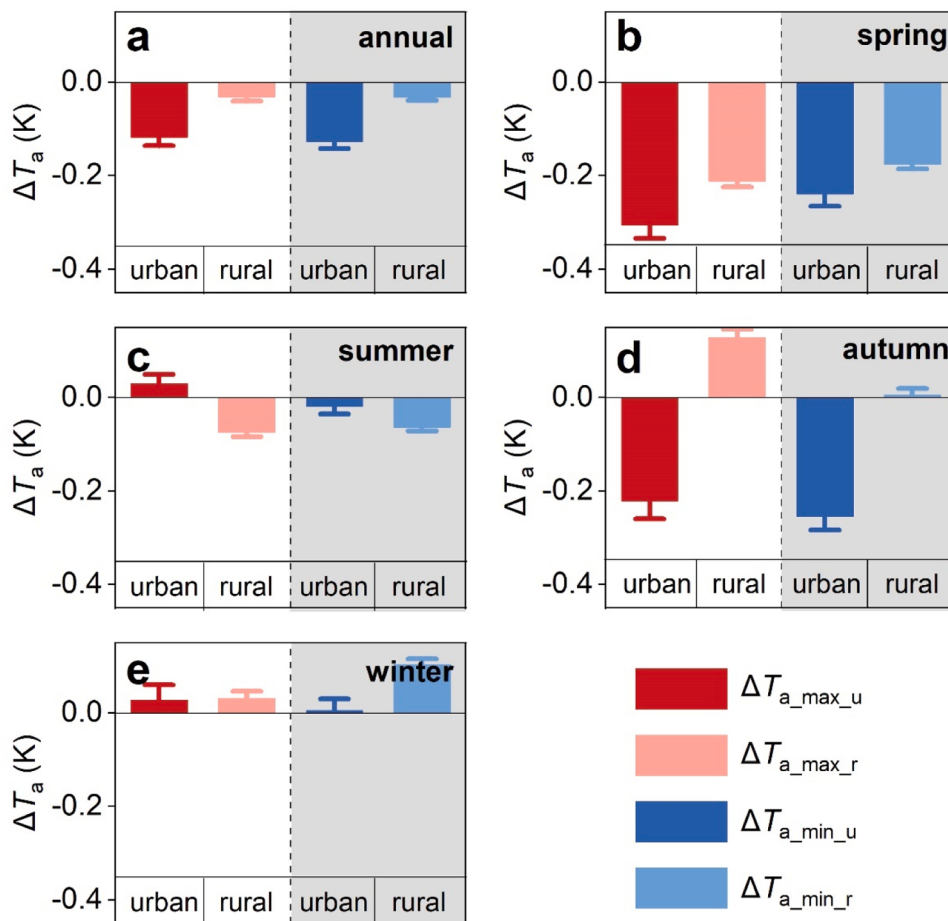


Fig. 3. Annual (a) and seasonal (b to e) variations of ΔT_a (i.e., the weekend effect of T_a) averaged for all selected cities, with the white and gray backgrounds representing the daytime and nighttime situations, respectively. $\Delta T_{a\text{max_u}}$, $\Delta T_{a\text{max_r}}$, $\Delta T_{a\text{min_u}}$, and $\Delta T_{a\text{min_r}}$ represent the ΔT_a for urban maximum T_a , rural maximum T_a , urban minimum T_a , and rural minimum T_a , respectively.

weekly rhythm during winter daytime (Fig. 5 and Fig. A7). The winter daytime ΔI_{ano_s} (i.e., I_s anomaly) averaged across all selected cities was positive from Monday to Wednesday while negative from Thursday to Sunday, with its maximum and minimum recorded on Monday (0.07 K) and Saturday (-0.06 K), respectively (Fig. 5b). The ΔI_s (i.e., difference in I_s between weekends and weekdays) was -0.06 K, and approximately 53% of the cities were identified by a negative ΔI_s (Fig. 5a). We speculate that such less pronounced weekly rhythms in global I_s when compared with its I_c counterpart may be related to the relatively lower sensitivity of I_s to human activity-induced AHR reduction (Liu et al., 2022; Oke et al., 2017). Besides, the greater limitations inherent in satellite-derived T_s observations in contrast to *in-situ* T_a measurements may also preclude the accurate monitoring of this phenomenon for I_s (refer to Section 4.3.1 for details).

We further observed a negative correlation between winter daytime ΔI_s and urban surface ISP across global cities (Fig. 5c). The ΔI_s displayed a value of -0.08 K over highly urbanized surfaces (i.e., ISP > 0.75) and -0.04 K over low ISP surfaces (i.e., ISP < 0.125). The ΔI_s also exhibited notable spatial variations across diverse climate zones (Fig. 5d and e). The most evident reduction in I_s during weekends was observed in cold climates (-0.24 K), followed by arid (-0.09 K) and warm climates (-0.03 K). However, equatorial climates demonstrated an insignificantly positive ΔI_s of 0.005 K (Fig. 5d). Besides, the ΔI_s was significantly negative in Asian (-0.09 K) and North American cities (-0.09 K) while was slightly positive across Oceanian cities (0.02 K) (Fig. 5e).

4.3. Uncertainty analysis

4.3.1. Uncertainties related to the data accuracy of T_a and T_s observations

4.3.1.1. *Uncertainties related to the data accuracy of in-situ T_a measurements.* One might argue that the observation error of *in-situ* T_a measurements (about 0.1 K; Cao et al., 2016) is comparable to our quantified ΔI_c . However, a more thorough sensitivity analysis, as elaborated in Section 3.3, revealed that the ΔI_c quantified using daily T_a time series perturbed by random errors aligns closely with the original findings (Fig. 6a and b). This suggests that the impacts from observation error of *in-situ* T_a observations on ΔI_c are negligible. This phenomenon can be explained by the Bessel formula (refer to Section 3.3), which indicates that the impacts from observation errors manifested at the per-station level can be considerably mitigated by the multiple averaging processes of random samples (Wang et al., 2022a). In our present investigation, for each station, we first quantified the weekend effect of *in-situ* T_a by averaging all weekend and weekday T_a over the study period. This temporal averaging procedure could significantly mitigate the impact from random errors of T_a measurement on the weekend effect of T_a for individual observations. Furthermore, our primary focus was on analyzing the ΔI_c patterns at global or regional scales, which entails averaging the weekend effects of T_a across numerous cities. Such spatial averaging procedures could further diminish the impact from random errors of T_a measurement at individual stations.

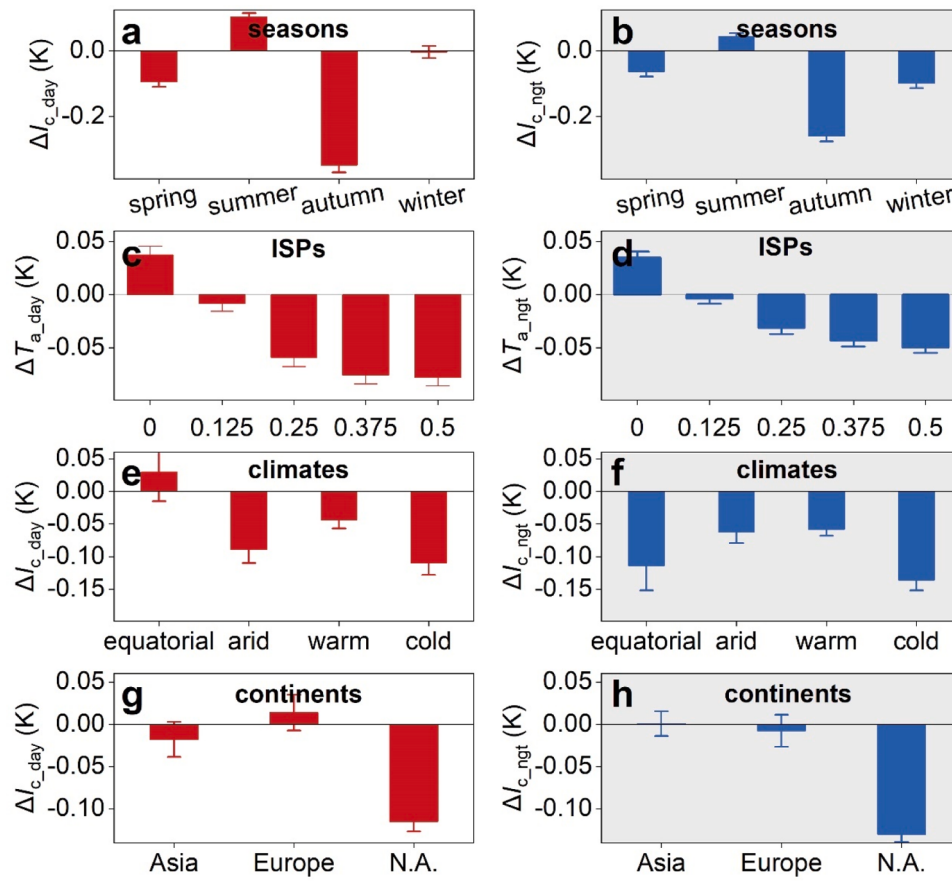


Fig. 4. Spatiotemporal variations of ΔI_c across all selected cities | The seasonal variations of global mean ΔI_c (a and b); ΔT_a variations along with ISP on a global scale (c and d); ΔI_c averaged for cities in various climates (e and f) and continents (g and h). The left column denotes the daytime situation while the right column represents the nighttime situation.

4.3.1.2. Uncertainties associated with the data accuracy of satellite T_s observations. For ΔI_s , practitioners may raise concerns that the retrieval error of satellite-derived T_s observations (about 1 K in most cases; Wan, 2013) could be larger than our quantified ΔI_s for winter daytime. However, our sensitivity analysis further showed that the impacts from T_s retrieval error on ΔI_s are relatively minimal (Fig. 6c), which could also be explained by the Bessel formula.

Nevertheless, our results demonstrated that the I_s only displayed notable weekly rhythms during winter daytime. In addition to the intrinsic causes that the I_s itself is less sensitive to AHR changes than the I_c (Liu et al., 2022; Oke et al., 2017), the greater data deficiencies of satellite-derived T_s observations compared to *in-situ* T_a measurements may also contribute to the less pronounced weekly phenomenon for I_s . Although we have adopted relatively stringent quality control procedures for T_s observations (refer to Section 3.2), it remains very difficult to fully compensate for their inherent limitations. Firstly, the T_s retrieval error can be significantly larger than its widely claimed magnitude of 1.0 K over highly heterogeneous urban surfaces that our study focuses on (Li et al., 2013), which represents a magnitude more than ten times larger than that of *in-situ* T_a measurements. Though the accuracy of T_s observations is flagged by quality control band, these flags can be significantly confounded by cloud contaminations (Jin & Dickinson, 2010; Li et al., 2013). Secondly, satellite T_s observations are susceptible to missing pixels due to cloud contaminations (Liao et al., 2022; Zhou et al., 2019), especially in urban areas. Thirdly, satellite-derived T_s over urban surfaces are often characterized by strong anisotropy due to varying sensor viewing angles and the complex geometry of urban canyons (Bian et al., 2024; Hu, Monaghan, Voogt & Barlage, 2016; Wang, Chen, Hu, Voogt & He, 2022b). Our sensitivity analyses further

showed that, as the quality of the used satellite T_s data has improved, the quantified ΔI_s became more evident (Fig. 7a), and its standard deviation significantly decreased (Fig. 7b). These strongly suggest that the magnitude of the captured weekly I_s signals is closely tied to the quality of T_s observations. Thus, it is important to note that our findings regarding the weekly rhythms of I_s may exist some potential uncertainty and they should be interpreted cautiously by practitioners. Nevertheless, the apparent increase in ΔI_s magnitude along with urban ISP across global cities, as clearly evidenced in this study (Fig. 5c), unequivocally provide strong evidence that the weekly schedules of human activities within cities indeed exert a nonnegligible influence on I_s . According to our findings as well as previous evidence that AHR can exert a more pronounced impact on I_s than on I_c (Liu et al., 2022), we can reasonably infer that if the data accuracy of T_s observations is comparable to that of T_a measurements, the weekly rhythms of I_s may be more evident than currently observed, yet these values should be less evident than those of the I_c .

4.3.2. Uncertainties related to the impacts from daily weather variations and official holidays

Our results indicated that daily weather variations had a minimal impact on the overall patterns of weekly rhythms of I_c (Fig. 8). Specifically, the impacts from daily weather variations on global mean ΔI_c was found to fluctuate within a very narrow range, spanning from -0.007 K to 0.007 K during the day and from -0.006 K to 0.007 K at night. These values only account for approximately 7% of the overall observed ΔI_c values (-0.09 K for daytime and -0.10 K for nighttime). Besides, all countries worldwide have their distinct free days, which may influence the division of weekends and weekdays, and thus bias the investigation

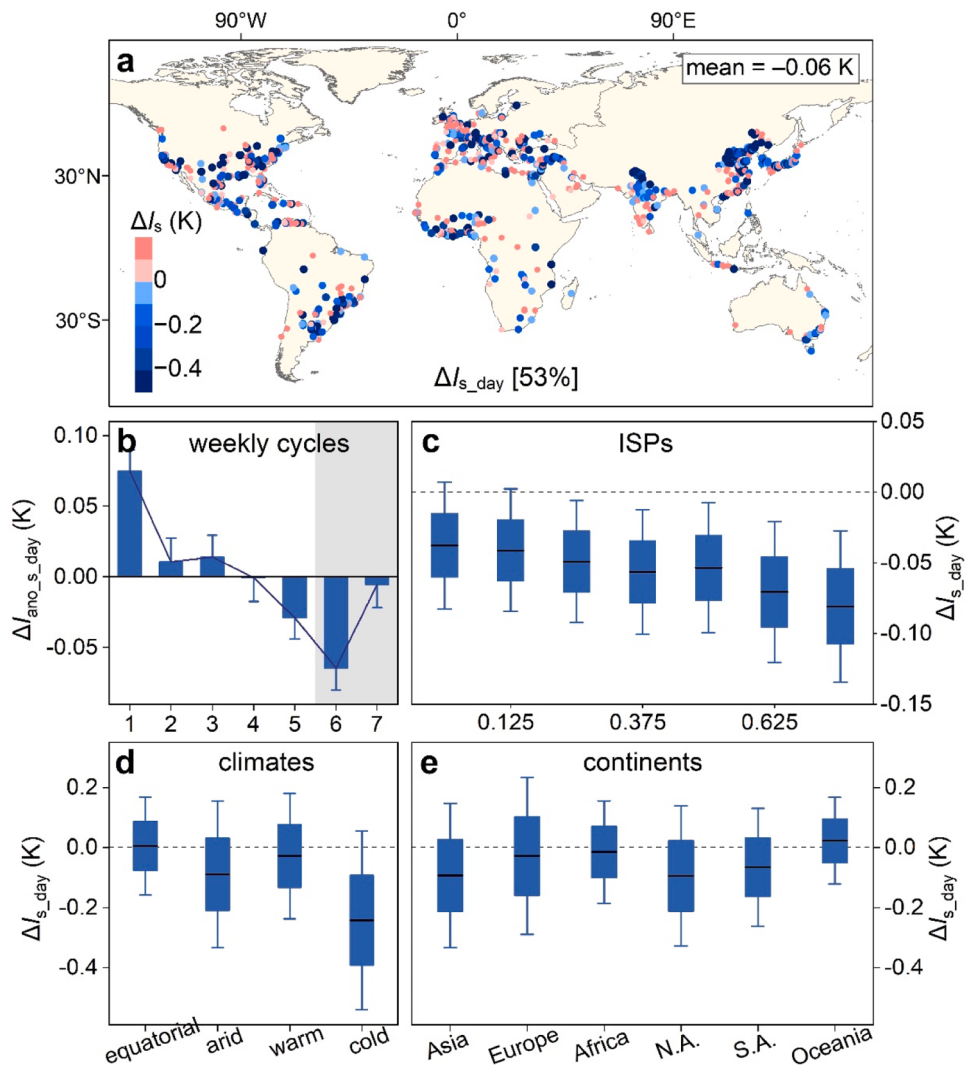


Fig. 5. Spatiotemporal variations of winter daytime ΔI_s across all selected cities | Spatial pattern of ΔI_s during winter daytime (a); weekly rhythms of winter daytime ΔI_s (denoted by I_s anomaly, termed ΔI_{ano_s} ; b); ΔI_s dynamics along with urban surface ISPs (c); ΔI_s across various climate zones (d) and continents (e). The numbers of 1 to 7 within (b) denote Monday to Sunday, and the N.A. and S.A. in (e) are abbreviations for North America and South America, respectively.

of weekly rhythms of UHIs. Yet our closer investigation revealed that the ΔI_c quantified with or without removing official holidays remain largely consistent both during the day and at night (Fig. 9). These indicate that the involvement of official holidays would not invalidate the investigation of the weekly rhythms of UHIs, which could be attributed to the fact that these holidays only account for a very small proportion of the overall study period (i.e., 5 years).

5. Discussion

5.1. Potential causes of the weekly rhythms of UHI

One may dispute that the weekly rhythm of UHI is an accidental phenomenon that caused by factors coincidentally projected onto the weekly cycle (e.g., background climate change, urbanization-induced land cover change, observation error of T_a measurements, and daily weather variations). However, both background climate change and urbanization-induced land cover change are gradual processes and they barely change over the short-term scale (Oke et al., 2017), so these factors are unlikely to account for such a weekly phenomenon. Furthermore, we also ruled out the impacts from both T_a observation error and daily weather variations through sensitivity analyses (refer to

Section 4.3). Therefore, the observed weekly rhythms of global UHIs are anticipated to be triggered by the regular weekly schedules of human activities.

To our knowledge, the reduction in human activity during weekends can lead to a decrease in both AHR and aerosols (i.e., particulate matter) (Earl et al., 2016; Forster & Solomon, 2003). The reduction in AHR is well known to weaken the UHI (Liu et al., 2022), while aerosols, owing to their complex direct and indirect mechanisms (Oke et al., 2017), can exert either positive or negative impacts on the UHI. Specifically, aerosols can reduce the shortwave radiation reaching the Earth's surfaces through scattering and absorption, thereby directly influencing the UHI. Aerosols can also involve the formation of cloud condensation nuclei and alter cloud amount and lifetime, thus inducing an indirect impact on the UHI (Jin, Shepherd & King, 2005; Oke et al., 2017). These imply that the weekly rhythms of global UHIs are likely to be co-regulated by the variations in both AHR and aerosols. For cities characterized by negative ΔI_c , it appears that the AHR-induced decline in UHI play a more dominant role than aerosols; yet for cities experiencing positive ΔI_c (i.e., some European cities; Fig. 2), this is likely because the aerosol-induced I_c increase outweighs the AHR-induced I_c reduction.

Nevertheless, it is important to note that the quantitative isolation of

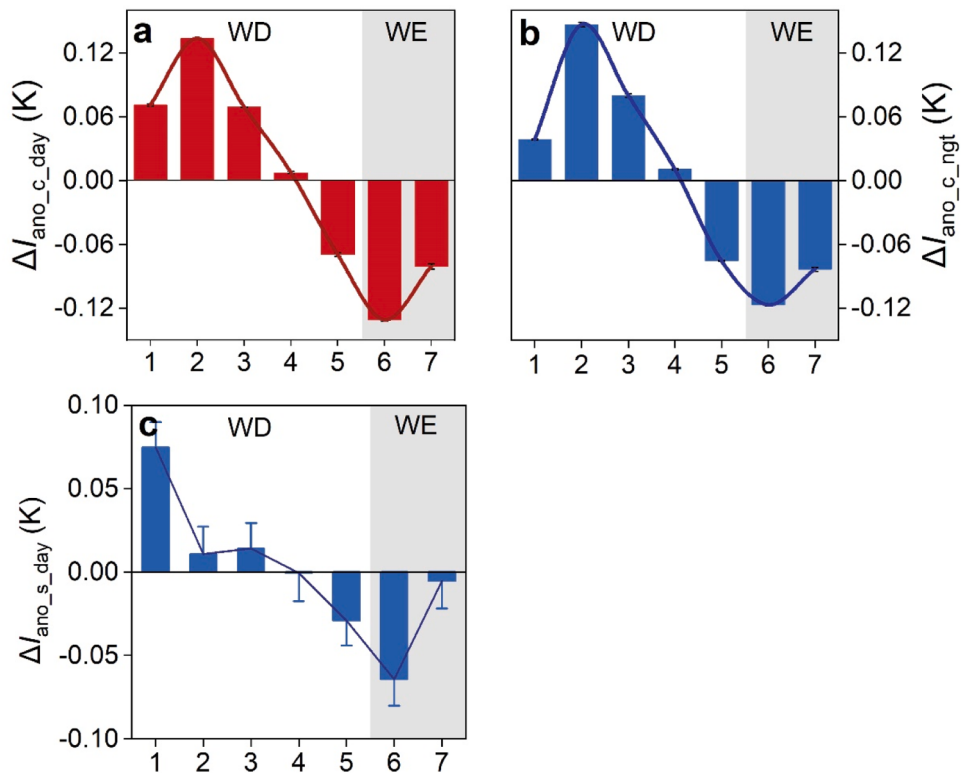


Fig. 6. Impacts from observation error of T_a and T_s observations on the quantification of weekly rhythms of canopy and surface UHIs | Weekly rhythms of canopy UHI quantified based on T_a observations perturbed by T_a observation error during the day (a) and at night (b); Weekly rhythms of surface UHI quantified based on T_s observations perturbed by T_s retrieval error during winter daytime (c).

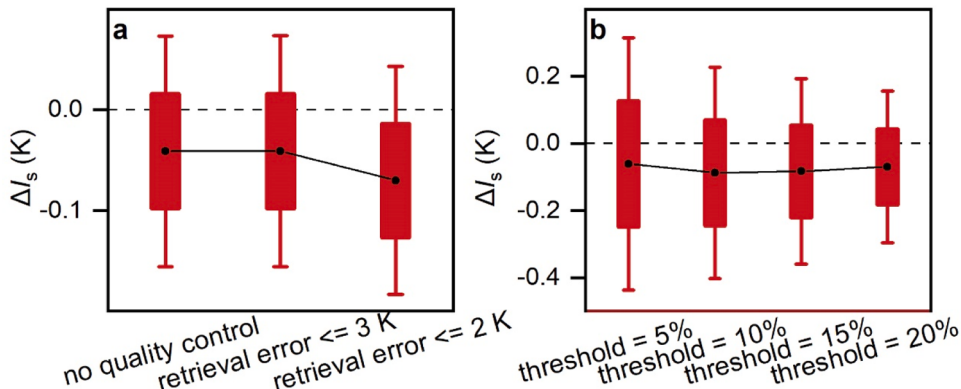


Fig. 7. Impacts from retrieval error (a) and missing data rates (b) of satellite T_s observations on the quantification of global mean winter daytime ΔI_s .

the individual contributions from AHRs and aerosols to the weekly rhythms of UHIs represents a formidable challenge, mostly for the following two reasons. First, the disentanglement of these isolated impacts necessitates examining the weekly rhythms of both AHR and aerosols across global cities; however, the daily AHR data remain unavailable even at regional scales (Jin et al., 2019; Yang et al., 2017). Besides, the determination of the relative magnitudes of positive and negative impacts of aerosols themselves is also intricate. It often relies on atmospheric physical models that are computationally intensive and require accurate input parameters (Andreae & Rosenfeld, 2008; Carslaw et al., 2010), making it rather difficult to obtain absolute statements regarding these impacts. Such a task becomes even harder when further considering the complex interactions between aerosols and UHI (Jin et al., 2010). Future endeavors remain essential to further untangle the underlying physical causes governing the weekly rhythms of global

UHIs.

5.2. Implications and limitations

This study documented a prevalent decline in I_c during weekends across global cities, as evidenced by the ΔI_c of -0.09 K and -0.10 K during the day and at night, respectively (Fig. 2). These findings suggested a potential decrease in global mean AHR by about $12\text{ W}\cdot\text{m}^{-2}$, given that an AHR reduction of $100\text{ W}\cdot\text{m}^{-2}$ generally corresponds to a decrease in I_c of 0.8 K (Oke et al., 2017). Although the human activity reductions during weekends are less pronounced compared to those during the Chinese Spring Festival and COVID-19 lockdown (Liu et al., 2022; Zhan et al., 2022), they hold the capacity to exert a non-negligible influence on the urban surface energy budget. By this way, our study contributes to a better understanding of global urban climate changes

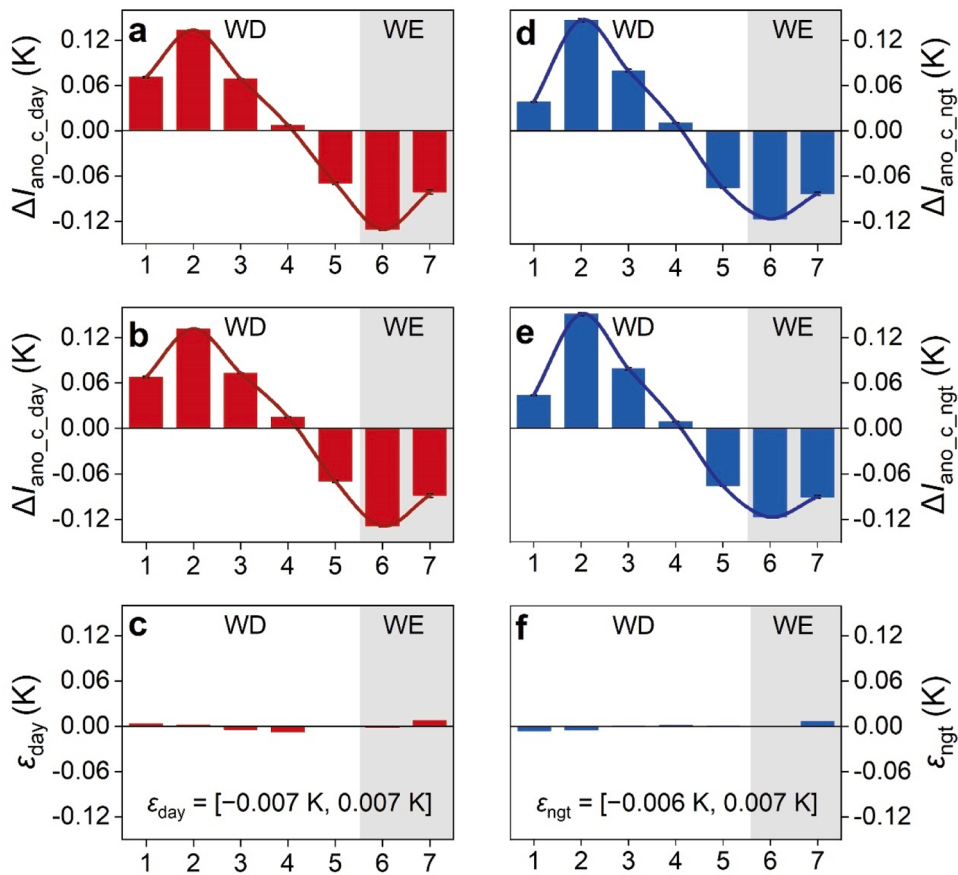


Fig. 8. Impacts from daily weather variabilities on the weekly rhythms of I_c (i.e., ΔI_{ano_c}) | The global annual mean daytime and nighttime ΔI_{ano_c} (termed $\Delta I_{ano_c_day}$ and $\Delta I_{ano_c_nigt}$, respectively) calculated based on original T_a time series (a and d) and based on newly generated T_a time series (b and e), as well as the ΔI_{ano_c} differences between these two time series (termed ε_{day} and ε_{nigt} , respectively; c and f).

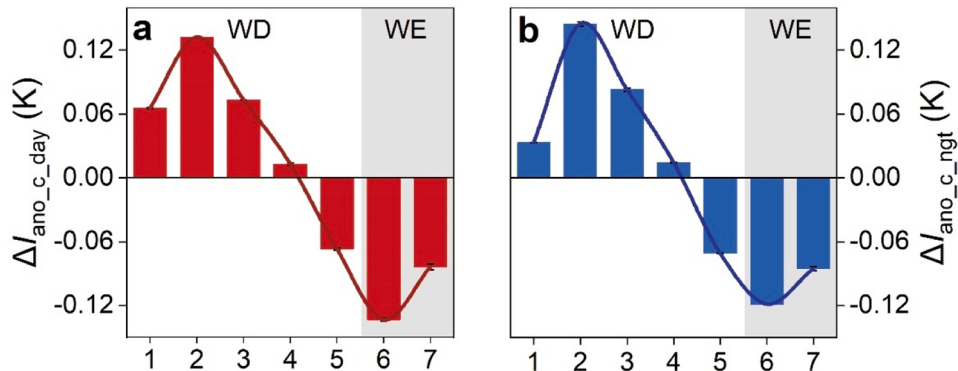


Fig. 9. Impacts from the involvement of free days on the examination of weekly rhythms of I_c | Weekly rhythms of I_c quantified with removing official holidays from weekdays, with (a) denoting the daytime case and (b) denoting the nighttime case.

caused by short-term cycles of human activities. This study demonstrated that the more pronounced reductions in both I_c and I_s were prone to occur over surfaces characterized by higher ISPs (Fig. 4c and d; Fig. 5c). These urban surfaces with higher ISP often coincide well with city central zones and experience larger population heat exposure due to the higher temperature and population density. Our findings may indicate the uneven impacts from human activities on intra-city microclimates. Besides, this study suggests that the UHI increment during weekends in a portion of global cities may be a combined result of AHR and aerosol variations, which highlights the potential significance of aerosols in projecting future global urban climates.

There are several limitations to our current study. Firstly, the uneven distribution of the selected cities used for ΔI_c quantification may introduce possible uncertainties into the associated results due to the insufficient representativity of global cities, particularly in equatorial regions. However, obtaining densely and evenly distributed weather stations equipped with high-quality daily T_a measurements across global cities is extremely difficult, and it has remained an enduring challenge within the urban climate community (Stewart, 2011). Secondly, the ΔI_c quantification may also be influenced by the exact locations of the chosen urban and rural stations. One recent study revealed that the impacts stemming from the spatial sampling of weather stations

becomes negligible once hundreds of cities are incorporated into the analysis (Du et al., 2021). This may suggest that the ΔI_c values obtained in this study at the regional and global scales should be less insensitive to the location of urban and rural stations and they can be considered reliable. Nevertheless, further rigorous theoretical analysis remains imperative. Thirdly, considering that the monitoring of such a subtle weekly signal requires mitigating the impact from daily temperature fluctuations through extensive averaging processes of adequate T_a observations, our study solely investigated the weekly rhythms of UHI at annual and seasonal timescales. Future endeavors should aim to examine these weekly signals at finer resolutions (e.g., per-month or per-week scales) using abundant T_a observations within individual cities. Moreover, beyond weekly rhythms, the UHI also demonstrates other short-term phenomenon such as that during the Spring Festival and COVID-19 lockdown period (Liu et al., 2022; Zhan et al., 2022). Future efforts will delve into exploring other holiday effects (e.g., National Day or Christmas) of UHIs to better disentangle urban climate changes induced by short-term human movements within cities.

6. Conclusion

This study investigated the weekly rhythms of both I_c and I_s from a multicity perspective, by integrating daily *in-situ* T_a measurements from >17,000 weather stations with satellite-derived T_s observations worldwide. The results indicate that: Firstly, the weekly rhythms of I_c averaged across all selected cities exhibit an evident peak–valley pattern in most seasons. In contrast, the weekly rhythm of I_s is only pronounced during winter daytime. These findings bridge a significant knowledge gap regarding the weekly rhythms of both canopy and surface UHIs on a large spatial scale. Secondly, the annual mean I_c reduction during weekends is 0.09 K during the day and 0.10 K at night, with the impacts from observation error of *in-situ* T_a observations on these values being less than 1%. These I_c reductions correspond to an AHR reduction of approximately 12 W m^{-2} , providing strong observational evidence for noticeable modifications of short-term population movements to urban climates. Thirdly, the reductions in both I_c and I_s during weekends

exhibit an inclination to escalate with urban ISP within cities, implying an uneven impact from human activities on intra-city urban climates. Our study illustrates the importance of short-term human mobility in shaping urban climates, and the associated findings may help develop more appropriate climate adaptation policies.[Fig. A1](#),[Fig. A2](#),[Fig. A3](#),[Fig. A4](#),[Fig. A5](#),[Fig. A6](#),[Fig. A7](#)

CRediT authorship contribution statement

Huilin Du: Data curation, Formal analysis, Investigation, Visualization, Writing – original draft. **Wenfeng Zhan:** Conceptualization, Funding acquisition, Methodology, Supervision, Writing – review & editing. **Zihan Liu:** Writing – review & editing. **Chunli Wang:** Writing – review & editing. **Shasha Wang:** Writing – review & editing. **Long Li:** Writing – review & editing. **Jiufeng Li:** Writing – review & editing. **Benjamin Bechtel:** Writing – review & editing. **Panagiotis Sismanidis:** Writing – review & editing.

Declaration of competing interest

The authors declare that they have no known competing financial interests or personal relationships that could have appeared to influence the work reported in this paper.

Data availability

Data will be made available on request.

Acknowledgments

We gratefully acknowledge the National Natural Science Foundation of China (42171306 and 42201337) for providing support for this current study. We also thank the support from the National Youth Talent Support Program of China.

Appendix

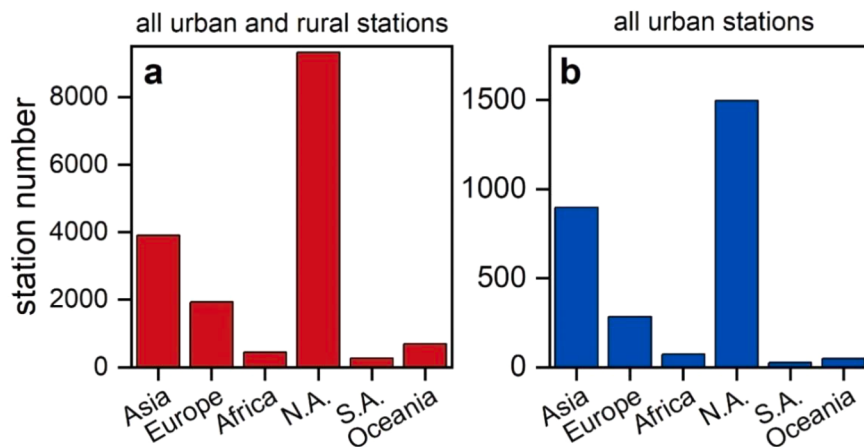


Fig. A1. The number of all stations (a) and urban stations (b) across different continents. The N.A. and S.A. are abbreviations for North America and South America, respectively.

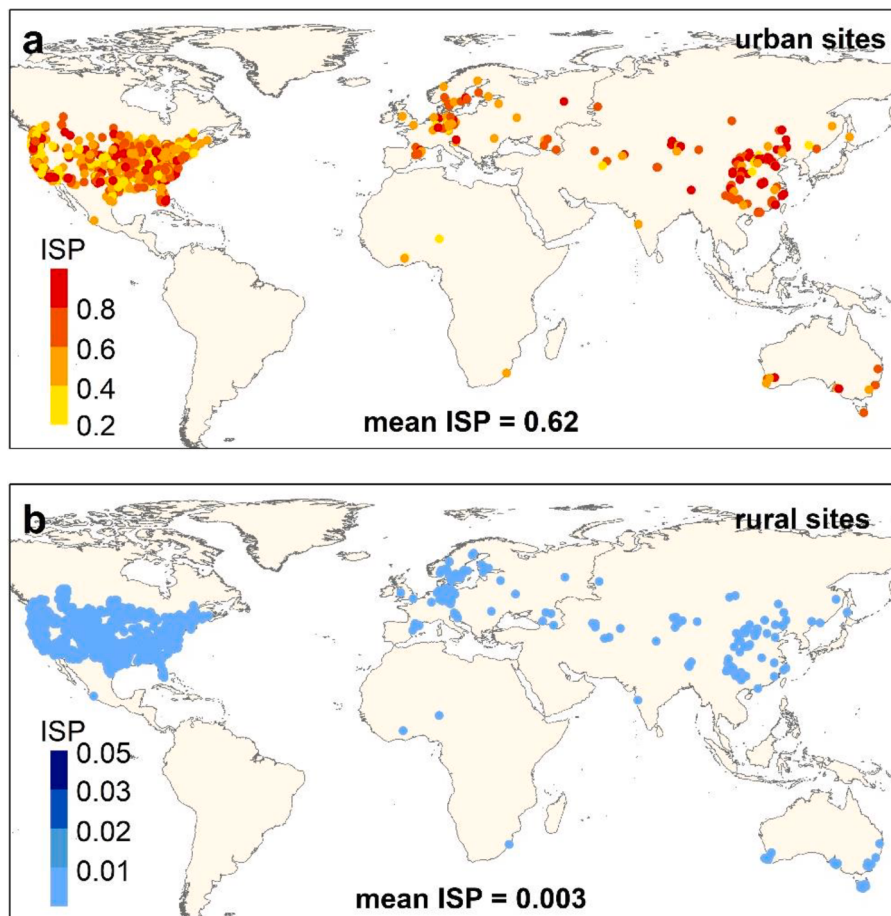


Fig. A2. Distribution of the chosen 1068 urban stations (a) and 1884 rural stations (b) as well as their impervious surface percentages (ISPs) of the surrounding 1-km buffer zones.

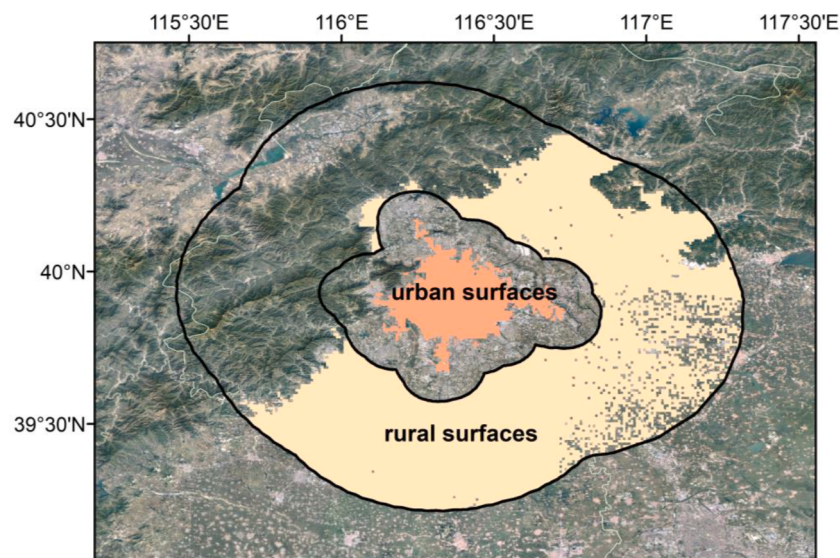


Fig. A3. Definitions of urban and rural surfaces in this study, taking Beijing, China, as an illustrated example.

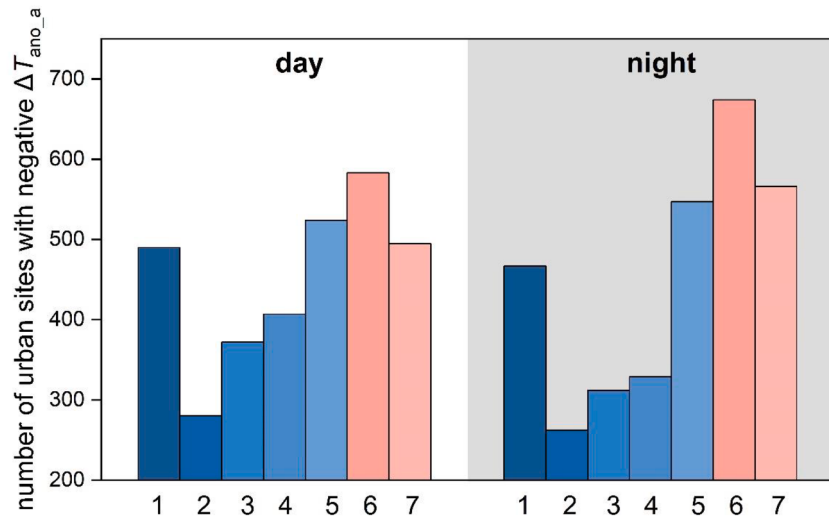


Fig. A4. Number of urban sites characterized by a negative $\Delta T_{\text{ano_a}}$ (i.e., daily T_a minus the weekly mean) within a weekly cycle. Number 1 to 7 denote Monday to Sunday, respectively.

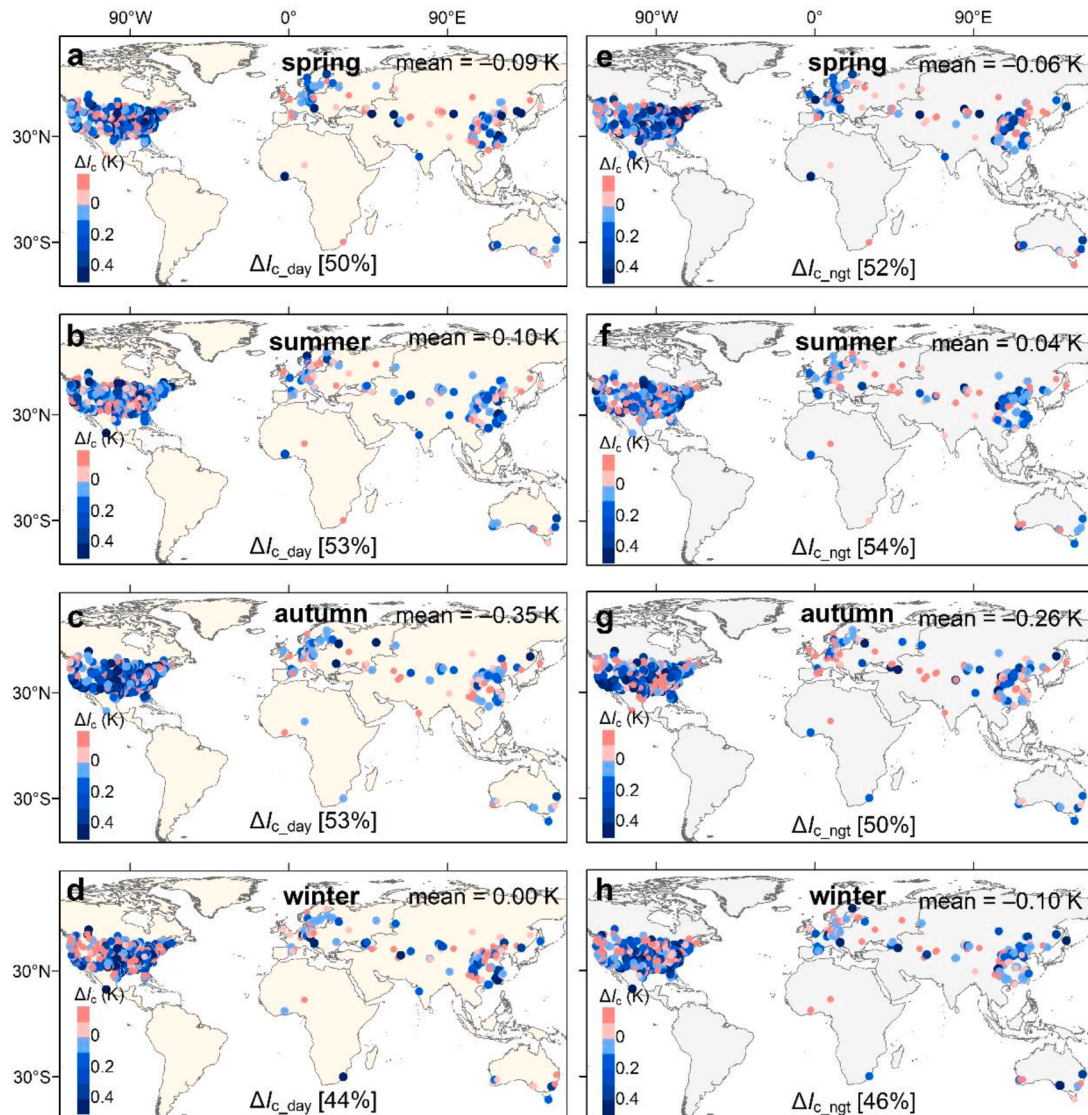


Fig. A5. Spatial patterns of ΔI_c across all selected cities during the daytime (ΔI_c_{day} ; a to d) and at night ($\Delta I_c_{\text{night}}$; e to h) for four seasons, with the percentages within parentheses denoting the proportion of cities with a negative ΔI_c .

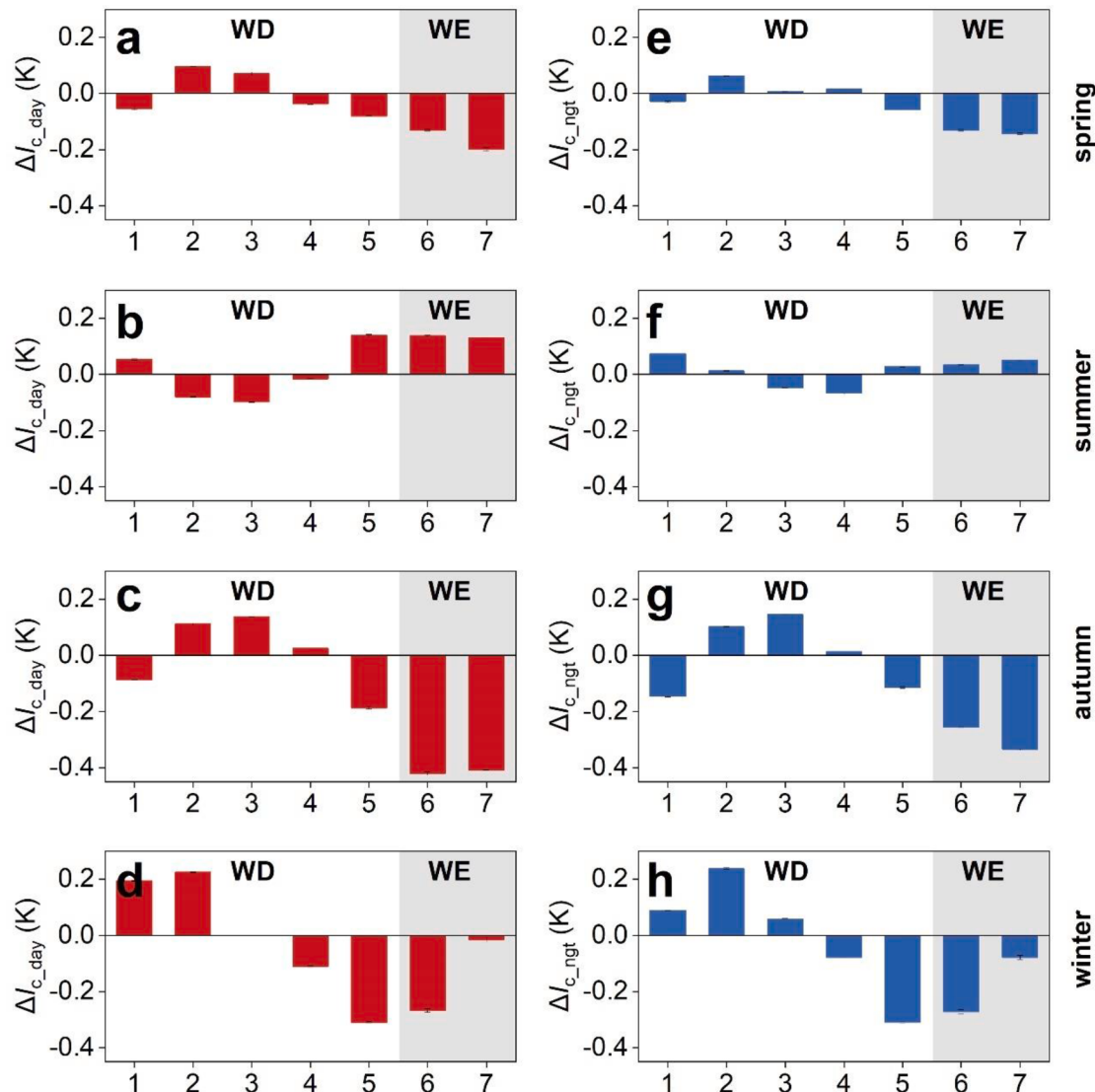


Fig. A6. Weekly rhythms of global mean I_c (denoted by I_c anomaly, termed $\Delta I_{ano,c}$) during the daytime ($\Delta I_{ano,c_day}$; a to d) and at night ($\Delta I_{ano,c_night}$; e to h) across four seasons. WE and WD are abbreviations for weekends and weekdays respectively, and the number of 1 to 7 denotes Monday to Sunday.

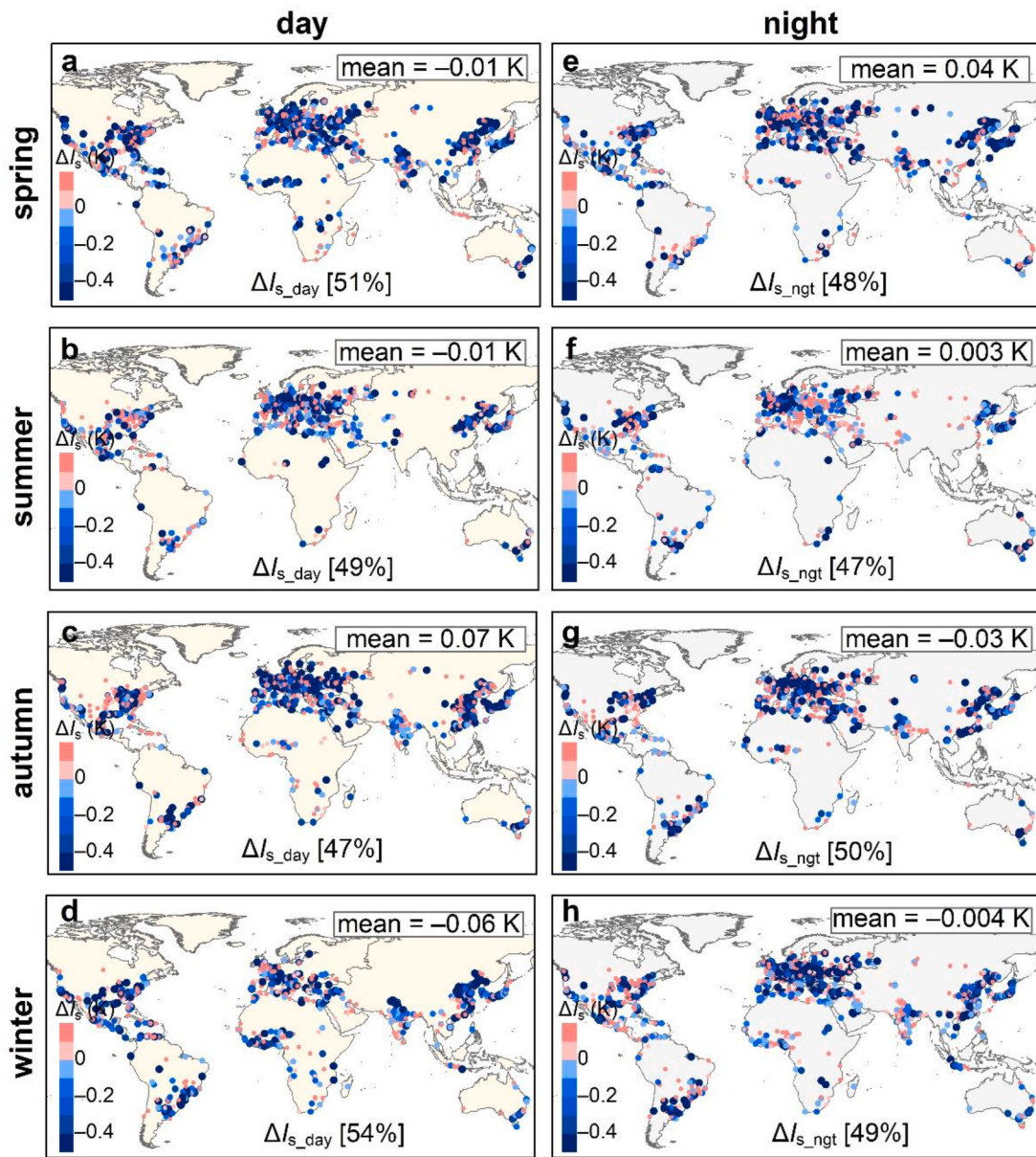


Fig. A7. The same as Fig. A5, but for I_s .

References

- Andreae, M. O., & Rosenfeld, D. (2008). Aerosol-cloud-precipitation interactions. Part 1. The nature and sources of cloud-active aerosols. *Earth-Science Reviews*, 89, 13–41.
- Bian, Z. J., Fan, T. Y., Roujean, J. L., Wang, D. D., Irvine, M., Wu, S. B., Cao, B., Li, H., Du, Y. M., & Xiao, Q. (2024). An analytical urban temperature model with building heterogeneity using geometric optical theory. *Remote Sensing of Environment*, 301, Article 113948.
- Bonamente, M. (2017). *Statistics and analysis of scientific data*. Springer.
- Buizza, R., Milleer, M., & Palmer, T. N. (1999). Stochastic representation of model uncertainties in the ECMWF ensemble prediction system. *Quarterly Journal of the Royal Meteorological Society*, 125, 2887–2908.
- Cao, L. J., Zhu, Y. N., Tang, G. L., Yuan, F., & Yan, Z. W. (2016). Climatic warming in China according to a homogenized data set from 2419 stations. *International Journal of Climatology*, 36, 4384–4392.
- Carlaw, K., Boucher, O., Spracklen, D., Mann, G., Rae, J., Woodward, S., & Kulmala, M. (2010). A review of natural aerosol interactions and feedbacks within the Earth system. *Atmospheric Chemistry and Physics*, 10, 1701–1737.
- Chakraborty, T., & Lee, X. H. (2019). A simplified urban-extent algorithm to characterize surface urban heat islands on a global scale and examine vegetation control on their spatiotemporal variability. *International Journal of Applied Earth Observation and Geoinformation*, 74, 269–280.
- Cryer, J. D., & Chan, K. S. (2008). *Time series analysis: With applications in r*. Springer.
- Du, H. L., Zhan, W. F., Liu, Z. H., Li, J. F., Li, L., Lai, J. M., Miao, S. Q., Huang, F., Wang, C. G., & Wang, C. L. (2021). Simultaneous investigation of surface and canopy urban heat islands over global cities. *ISPRS Journal of Photogrammetry and Remote Sensing*, 181, 67–83.
- Du, H. L., Zhan, W. F., Voogt, J., Bechtel, B., Chakraborty, T. C., Liu, Z. H., Hu, L. Q., Wang, Z. H., Li, J. F., Fu, P., Liao, W. L., Luo, M., Li, L., Wang, S. S., Huang, F., & Miao, S. Q. (2023). Contrasting trends and drivers of global surface and canopy urban heat islands. *Geophysical Research Letters*, 50.
- Earl, N., Simmonds, I., & Tapper, N. (2016). Weekly cycles in peak time temperatures and urban heat island intensity. *Environmental Research Letters*, 11.
- Elsayed, I. S. (2012). A study on the urban heat island of the city of Kuala Lumpur, Malaysia. *Journal of King Abdulaziz University*, 23, 121.
- Forster, P. M.d. F., & Solomon, S. (2003). Observations of a “weekend effect” in diurnal temperature range. *PNAS*, 100, 11225–11230.
- Friedl, M., & Sulla-Menashe, D. (2019). MCD12Q1 MODIS/Terra+ Aqua Land Cover Type Yearly L3 Global 500m SIN Grid V006. In *Proceedings of the 2019, distributed by NASA EOSDIS Land Processes DAAC*.
- Giachi, S., & Vallejo-Peña, A. (2022). Comparing flexible working hours in northern and southern Europe: A methodological analysis using individual survey data. *E-Journal of International and Comparative Labour Studies*, 11.

- Gong, D. Y., Guo, D., & Ho, C. H. (2006). Weekend effect in diurnal temperature range in China: Opposite signals between winter and summer. *Journal of Geophysical Research: Atmospheres*, 111.
- Gong, P., Li, X. C., Wang, J., Bai, Y. Q., Chen, B., Hu, T. Y., Liu, X. P., Xu, B., Yang, J., & Zhang, W. (2020). Annual maps of global artificial impervious area (GAIA) between 1985 and 2018. *Remote Sensing of Environment*, 236, Article 111510.
- Hart, M. A., & Sailor, D. J. (2009). Quantifying the influence of land-use and surface characteristics on spatial variability in the urban heat island. *Theoretical and Applied Climatology*, 95, 397–406.
- Hsu, A., Sheriff, G., Chakraborty, T., & Manya, D. (2021). Disproportionate exposure to urban heat island intensity across major US cities. *Nature Communications*, 12, 2721.
- Hu, L. Q., Monaghan, A., Voogt, J. A., & Barlage, M. (2016). A first satellite-based observational assessment of urban thermal anisotropy. *Remote Sensing of Environment*, 181, 111–121.
- Inhoff, M. L., Zhang, P., Wolfe, R. E., & Bounoua, L. (2010). Remote Sensing of the urban heat island effect across biomes in the continental USA. *Remote Sensing of Environment*, 114, 504–513.
- Jin, K., Wang, F., Chen, D. L., Liu, H. H., Ding, W. B., & Shi, S. Y. (2019). A new global gridded anthropogenic heat flux dataset with high spatial resolution and long-term time series. *Scientific Data*, 6, 139.
- Jin, M. L., & Dickinson, R. E. (2010). Land surface skin temperature climatology: Benefiting from the strengths of satellite observations. *Environmental Research Letters*, 5, Article 044004.
- Jin, M. L., Shepherd, J. M., & King, M. D. (2005). Urban aerosols and their variations with clouds and rainfall: A case study for New York and Houston. *Journal of Geophysical Research: Atmospheres*, 110.
- Kamma, J., Manomaiphiboon, K., Aman, N., Thongkamdee, T., Chuangchote, S., & Bonnet, S. (2020). Urban heat island analysis for Bangkok: Multi-scale temporal variation, associated factors, directional dependence, and cool island condition. *Science Asia*, 46.
- Lai, J., Zhan, W., Huang, F., Quan, J., Hu, L., Gao, L., & Ju, W. (2018). Does quality control matter? Surface urban heat island intensity variations estimated by satellite-derived land surface temperature products. *ISPRS Journal of Photogrammetry and Remote Sensing*, 139, 212–227.
- Li, X. C., Gong, P., Zhou, Y. Y., Wang, J., Bai, Y. Q., Chen, B., Hu, T. Y., Xiao, Y. X., Xu, B., & Yang, J. (2020). Mapping global urban boundaries from the global artificial impervious area (GAIA) data. *Environmental Research Letters*, 15, Article 094044.
- Li, Z. L., Tang, B. H., Wu, H., Ren, H. Z., Yan, G. J., Wan, Z. M., Trigo, I. F., & Sobrino, J. A. (2013). Satellite-derived land surface temperature: Current status and perspectives. *Remote Sensing of Environment*, 131, 14–37.
- Liao, Y., Shen, X., Zhou, J., Ma, J., Zhang, X., Tang, W., Chen, Y., Ding, L., & Wang, Z. (2022). Surface urban heat island detected by all-weather satellite land surface temperature. *The Science of the total environment*, 811, Article 151405.
- Liu, Z. H., Lai, J. M., Zhan, W. F., Bechtel, B., Voogt, J., Quan, J. L., Hu, L. Q., Fu, P., Huang, F., Li, L., Guo, Z., & Li, J. F. (2022). Urban heat islands significantly reduced by COVID-19 lockdown. *Geophysical Research Letters*, 49, Article e2021GL096842.
- Luo, M., & Lau, N. C. (2018). Increasing heat stress in urban areas of eastern China: Acceleration by urbanization. *Geophysical Research Letters*, 45, 13,060–013,069.
- Luo, M., & Lau, N. C. (2019). Urban expansion and drying climate in an urban agglomeration of East China. *Geophysical Research Letters*, 46, 6868–6877.
- Menne, M. J., Durre, I., Vose, R. S., Gleason, B. E., & Houston, T. G. (2012). An overview of the global historical climatology network-daily database. *Journal of Atmospheric and Oceanic Technology*, 29, 897–910.
- Ngarambe, J., Joen, S. J., Han, C. H., & Yun, G. Y. (2021). Exploring the relationship between particulate matter, CO, SO₂, NO₂, O₃ and urban heat island in Seoul. *Korean Journal of Hazardous Materials*, 403, Article 123615.
- Nwaerema, P., & Jiya, S. N. (2021). Evaluation of temperature and urban heat island variability in days of the week and weekends. *International Journal of Human Capital in Urban Management*, 6, 45–56.
- Oke, T. R. (1973). City size and the urban heat island. *Atmospheric environment*, 7, 769–779, 1967.
- Oke, T. R. (1982). The energetic basis of the urban heat island. *Quarterly Journal of the Royal Meteorological Society*, 108, 1–24.
- Oke, T. R. (2004). Initial guidance to obtain representative meteorological observations at urban sites. *IOM report no.81, WMO/TD. no.1250*. Geneva: World Meteorological Organization.
- Oke, T. R., Mills, G., Christen, A., & Voogt, J. A. (2017). *Urban climates*. Cambridge University Press.
- Papanastassiou, D. K., & Kittas, C. (2012). Maximum urban heat island intensity in a medium-sized coastal Mediterranean city. *Theoretical and Applied Climatology*, 107, 407–416.
- Peel, M. C., Finlayson, B. L., & McMahon, T. A. (2007). Updated world map of the Köppen-Geiger climate classification. *Hydrology and Earth System Sciences*, 11, 1633–1644.
- Peng, S. S., Piao, S. L., Ciais, P., Friedlingstein, P., Ottle, C., Breon, F. M., Nan, H. J., Zhou, L. M., & Myneni, R. B. (2012). Surface urban heat island across 419 global big cities. *Environmental Science & Technology*, 46, 696–703.
- Pugachev, V. S. (2014). *Probability theory and mathematical statistics for engineers*. Elsevier.
- Santamouris, M. (2014). On the energy impact of urban heat island and global warming on buildings. *Energy and buildings*, 82, 100–113.
- Shahmohamadi, P., Che-Ani, A., Maulud, K., Tawil, N. M., & Abdullah, N. (2011). The impact of anthropogenic heat on formation of urban heat island and energy consumption balance. *Urban Studies Research*, 2011.
- Shen, C., Hou, H., Zheng, Y., Murayama, Y., Wang, R., & Hu, T. (2022). Prediction of the future urban heat island intensity and distribution based on landscape composition and configuration: A case study in Hangzhou. *Sustainable Cities and Society*, 83, Article 103992.
- Song, X. P., Sexton, J. O., Huang, C. Q., Channan, S., & Townshend, J. R. (2016). Characterizing the magnitude, timing and duration of urban growth from time series of Landsat-based estimates of impervious cover. *Remote Sensing of Environment*, 175, 1–13.
- Stewart, I. D. (2011). A systematic review and scientific critique of methodology in modern urban heat island literature. *International Journal of Climatology*, 31, 200–217.
- Venter, Z. S., Chakraborty, T., & Lee, X. H. (2021). Crowdsourced air temperatures contrast satellite measures of the urban heat island and its mechanisms. *Science Advances*, 7, eabb9569.
- Wan, Z. M. (2013). *Collection-6 modis land surface temperature products users' guide*. University of California.
- Wang, C. L., Zhan, W. F., Liu, X. L., Liu, Z. H., Miao, S. Q., Du, H. L., Li, J. F., Wang, C. G., Li, L., & Yue, W. Z. (2022a). Strong modulation of human-activity-induced weekend effect in urban heat island by surface morphology and weather conditions. *Journal of Geophysical Research: Atmospheres*, Article e2022JD036905.
- Wang, D. D., Chen, Y. H., Hu, L. Q., Voogt, J. A., & He, X. Y. (2022b). Satellite-based daytime urban thermal anisotropy: A comparison of 25 global cities. *Remote Sensing of Environment*, 283, Article 113312.
- Wang, X. L. (2008). Penalized maximal F test for detecting undocumented mean shift without trend change. *Journal of Atmospheric and Oceanic Technology*, 25, 368–384.
- Wu, Y., Hou, H., Wang, R., Murayama, Y., Wang, L., & Hu, T. (2022). Effects of landscape patterns on the morphological evolution of surface urban heat island in Hangzhou during 2000–2020. *Sustainable Cities and Society*, 79, Article 103717.
- Yang, W. M., Luan, Y. B., Liu, X. L., Yu, X. Y., Miao, L. J., & Cui, X. F. (2017). A new global anthropogenic heat estimation based on high-resolution nighttime light data. *Scientific Data*, 4, 1–11.
- Yang, Y. J., Guo, M., Wang, L. L., Zong, L., Liu, D. Y., Zhang, W. J., Wang, M. Y., Wan, B. C., & Guo, Y. D. (2023). Unevenly spatiotemporal distribution of urban excess warming in coastal Shanghai megacity, China: Roles of geophysical environment, ventilation and sea breezes. *Building and Environment*, 235, Article 110180.
- Ye, X. M., Xiao, X. B., Shi, J. B., & Ling, M. (2016). The new concepts of measurement error theory. *Measurement*, 83, 96–105.
- Zahumenský, I. (2004). Guidelines on quality control procedures for data from automatic weather stations. *World Meteorological Organization, Switzerland*, 955, 2–6.
- Zhan, W. F., Liu, Z. H., Bechtel, B., Li, J. F., Lai, J. M., Fu, H. Y., Li, L., Huang, F., Wang, C. L., & Chen, Y. Y. (2022). Urban-rural gradient in urban heat island variations responsive to large-scale human activity changes during Chinese New Year holiday. *Geophysical Research Letters*, Article e2022GL100689.
- Zhang, H., Luo, M., Pei, T., Liu, X., Wang, L., Zhang, W., Lin, L., Ge, E., Liu, Z., & Liao, W. (2023). Unequal urban heat burdens impede climate justice and equity goals. *The Innovation*, 4, Article 100488.
- Zhang, L. R., Luo, F., Pan, G. T., Zhang, W. J., Ren, G. Y., Zheng, Z. F., & Yang, Y. J. (2024). Elucidating the multi-timescale variability of a canopy urban heat island by using the short-time Fourier transform. *Geophysical Research Letters*, 51, Article e2023GL106221.
- Zhang, P. F., Ren, G. Y., Qin, Y., Zhai, Y. Q., Zhai, T. L., Tysa, S. K., Xue, X. Y., Yang, G. W., & Sun, X. B. (2021). Urbanization effects on estimates of global trends in mean and extreme air temperature. *Journal of Climate*, 34, 1923–1945.
- Zhang, X., Liu, L. Y., Wu, C. S., Chen, X. D., Gao, Y., Xie, S., & Zhang, B. (2020). Development of a global 30m impervious surface map using multisource and multitemporal Remote Sensing datasets with the Google Earth Engine platform. *Earth System Science Data*, 12, 1625–1648.
- Zhao, L., Oppenheimer, M., Zhu, Q., Baldwin, J. W., Ebi, K. L., Bou-Zeid, E., Guan, K. Y., & Liu, X. (2018). Interactions between urban heat islands and heat waves. *Environmental Research Letters*, 13, Article 034003.
- Zhou, D. C., Sun, S. L., Li, Y., Zhang, L. X., & Huang, L. (2023). A multi-perspective study of atmospheric urban heat island effect in China based on national meteorological observations: Facts and uncertainties. *The Science of the Total Environment*, 854, Article 158638.
- Zhou, D. C., Xiao, J. F., Bonafoni, S., Berger, C., Deilami, K., Zhou, Y. Y., Frolking, S., Yao, R., Qiao, Z., & Sobrino, J. A. (2019). Satellite Remote Sensing of surface urban heat islands: Progress, challenges, and perspectives. *Remote Sensing*, 11, 48.